RSC Advances

ROYAL SOCIETY OF CHEMISTRY

www.rsc.org/advances

Effect of growth temperature on the optical properties of ZnO nano-structure grown by simple hydrothermal method

Rajasree Das[1,2†], Amit Kumar[1], Yogendra Kumar[2], Somaditya Sen[1,2] and Parasharam M. Shirage[1,2*]

[1]Department of Physics, Indian Institute of Technology Indore, Khandwa Road, Simrol Campus, Indore-452020. India

[2]Centre for Materials Science and Engineering, Indian Institute of Technology Indore, Khandwa Road, Simrol Campus, Indore-452020. India

* Corresponding author: E-mail: pmshirage@iiti.ac.in and paras.shirage@gmail.com (P. M. Shirage)

† E-mail: dasrajasree@gmail.com

ABSTRACT

Here we report an easy and rapid synthesis technique of wurtzite ZnO nano structures in the form of flowers, nano-rods and nano-tubes is achieved by a facile hydrothermal method. A growth mechanism is proposed based on series of temperature dependent experiments keeping other parameters during synthesis in the aqueous medium at optimized level. Pure ZnO results in nano-rods while Sr doped ZnO material forms flower and tube like structures. The XRD and TEM investigations show that ZnO nanostructures possess good crystalline structures with growth direction along the *c*-axis of the crystal plane. Raman spectra confirms five phonon vibration modes for ZnO nanostructures at 99, 333, 382, 438 and 582 cm^{-1} and one more defect induced low intensity peak at 663 cm^{-1} for Sr doped ZnO. Ultraviolet–visible (UV–vis) spectroscopy shows the band gap energy of ZnO nanostructures decreases from 3.24 to 3.22 eV with the substitution of Sr in ZnO lattice. Photoluminescence spectra reveal existence of several defect states in all the samples. Defect intensity seems negligibly affected by the variation of growth temperature, whereas, Sr doping plays a major role in controlling oxygen and Zn related defects. I-V characteristics of the ZnO and Sr doped ZnO shows rectification behaviour of the Schottky diodes.

1. Introduction

Nano-semiconductor materials have gained much more attention in recent years owing to their anticipated properties and applications in different areas such as photoelectron devices, sensors, catalysts,and photovoltaic devices *etc.* Nanomaterials have innovative optical, structural, electronic, and thermal properties which are of great scientific importance in basic and applied fields. Among these Zinc Oxide (ZnO) is one of the most important natural *n*-type semiconductor[1] with a direct wide band gap near-UV spectral region (3.36 eV at room temperature (RT))[2], large free exciton binding energy[3] of 60 meV making it suitable for RT excitonic emission processes[4]. All these properties of ZnO are promising for device fabrications in optoelectronics and photonics[1,5] including photo-detectors, transparent thin-film transistors, light emitting diodes (LED) *etc*. The optical and electrical properties of ZnO intensively depends on the structure, size, shape, defect concentration *etc*. which makes controlling growth and structure very important and interesting topic in recent material research fields.The most stable structure in ZnO is wurtzite structure, which is stable up to a high temperature range (~2000^{o}C). Wet chemical, electro-deposition, template assisted route, thermal evaporation, chemical vapor deposition (CVD) are commonly used and well known techniques for ZnO nanostructure growth. But most of these techniques either operates at high temperature or need sophisticated instruments. The simple and economically inexpensive technique among the aforementioned techniques is the hydrothermal method to prepare highly crystalline ZnO. Investigations focused on developing sophisticated nanoscale materials like nano-particles, nano-tubes, nano-wires, nano-rods, nano-sheets, nano-clusters, nano-cones *etc.* are still desirable due to their importance in device fabrication and other practical applications. Different complex ZnO nanostructures like ZnO nano-flowers[6], rotor-like microcrystals [7], spindle-like nanorods[8], hexagonal disks and rings[9], doughnut-shapedmicro-particles[10] *etc.* have been prepared following wet chemical synthesis route. In order to get these important morphologies use of microwave or auto-clave is unavoidable. The naturally the question arises is whether is it possible to get one of these morphologies by avoiding high temperature, microwave or autoclaves? To address this question we intentionally started to search for the methodology which provides many of the aforementioned morphologies with as excellent properties. Here, we present a simpler hydrothermal techniqueto grow ZnO nanostructure with excellent crystallinity. Formation of nano-rods are observed at low depositionand annealing temperatures whereas needle like nano-rod grows at high deposition temperature. Effect of growth

temperature on the alkaline metal, Sr doped ZnO, is also studied. We have studied the structural and optical properties of the pure and east studied Sr-doped ZnO nanomaterials and presented in this manuscript.

2. Experimental technique

Highly crystalline and single phase ZnO and $Zn_{0.98}Sr_{0.02}O$ nanostructures (nanorod, nano-flowers and nanotubes) on glass substrates are prepared by developing a most simple and inexpensive hydrothermal process in a large scale. An aqueous solution of Zn nitrate (Alfa Aesar) and strontium nitrate(Alfa Aesar) salts were prepared by adding the appropriate quantity of double distilled water. After few minutes of continuous stirring for uniform mixing and complete dissolution, the appropriate quantity of aqueous ammonia is added to maintain a pH ~ 12. Then well cleaned glass substrates dipped in the solution and solution heated at desired temperature. To understand the growth mechanism more clearly, reaction time is kept fixed (~60 min) while temperature is varied (100°C and 120°C). After the completion of the deposition, the ZnO deposited glass substrates were taken out and cleaned with double distilled water for several times and dried overnight in the air. Further to remove the hydroxides present in the films and to get phase pure ZnO nanostructure, annealed in air at different temperatures (150°C, 250°C and 350°C) for 2 hr. In the present investigation, sample naming is as follows:

		Annealing Temperature		
		150°C	***250°C***	***350°C***
ZnO film deposited at 100°C	→	ZnO1	ZnO2	ZnO3
ZnO film deposited at 120°C	→	ZnO4	ZnO5	ZnO6
$Zn_{0.98}Sr_{0.02}O$film deposited at 100°C	→	SrZnO1	SrZnO2	SrZnO3
$Zn_{0.98}Sr_{0.02}O$film deposited at 120°C	→	SrZnO4	SrZnO5	SrZnO6

The phase formation, composition and surface morphology of the ZnO and $Zn_{0.98}Sr_{0.02}O$ films were investigated by X-ray diffraction (XRD, Bruker D8 Advance X-ray diffractometer) with Cu-K_α radiation (λ= 1.54 Å) and field emission scanning electron microscope (FESEM, Supra 55 Zeiss). Micro Raman scattering measurement of the samples were recorded using Labram-HR 800 spectrometer equipped with excitation radiation at wavelength of 488 nm from an argon ion laser

at a spectral resolution of about 1 cm^{-1}. Optical band gap was determined with the diffused reflectance spectrometer (Agilent Cary-60 UV-Vis). Room temperature (RT) fluorescence spectroscopic measurements were conducted using a spectrofluorometer (Horiba Jobin Yvon, Fluorolog-3) having Xe lamp source with an excitation wavelength of 330 nm. The I-V characteristics of ZnO were measured by Keithley source meter 2401.

3. Results and Discussions:

Fig 1.(*A*) shows the XRD patterns of the ZnO and $Zn_{0.98}Sr_{0.02}O$ nanostructure deposited at 120°C temperature and annealed at 350°C temperature and *Fig 1. (B)* shows XRD pattern of undoped ZnO films deposited and annealed at different temperatures. All major XRD peaks of the films can be indexed to the hexagonal phase of wurtzite ZnO (space group *P63mc*)[11, 12] suggesting that all the films are phase pure except a very low intensity peak nearby $2\theta = 31.0^{o}$, observed for ZnO1 films which corresponds to the $Zn(OH)_2$ impurity peak. The XRD pattern shows the high intensity peak of (002) in all the samples, which indicates that films are preferentially oriented along (00*l*) plane. Inset of Fig 1(*A*) shows the change in peak position towards lower diffraction angle in the Sr doped film. Atomic radius of Sr^{+2} (0.118 nm) is larger in comparison to Zn^{+2}(0.074 nm), therefore Sr doping at Zn increases the lattice size in the $Zn_{0.98}Sr_{0.02}O$ film, resulting a decrease in the diffraction angle. Inset of Fig 1(*B*). shows that lattice parameter (*a* and *c*) value is almost same in the undoped films whereas increases in the SrZnO6 film which justifies the decrease in diffraction angle in Sr doped film.

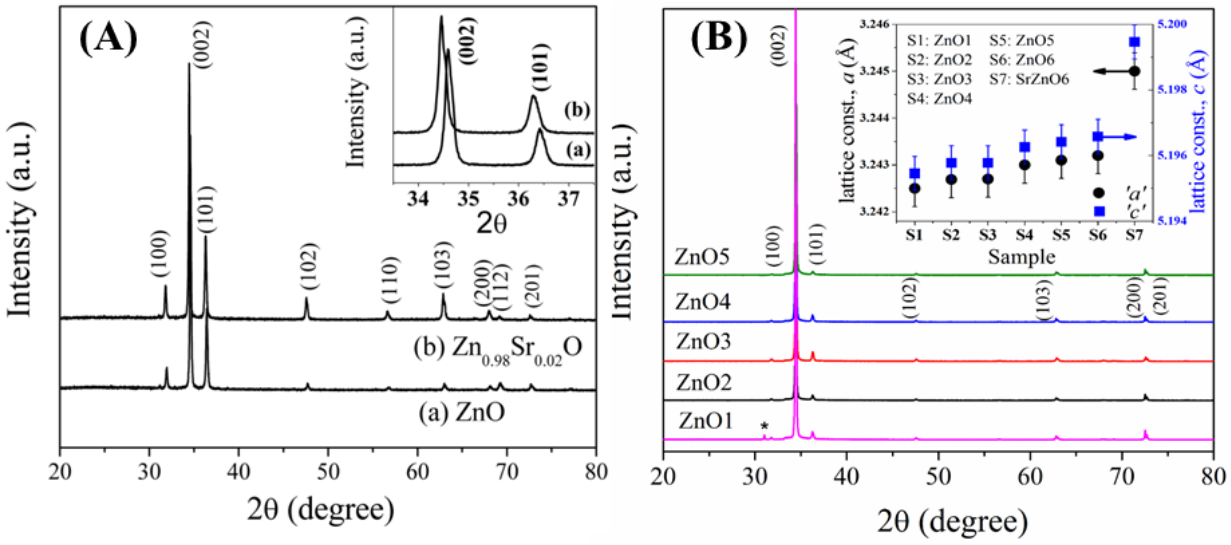

Fig. 1. (Color online) (A) XRD patterns of (*a*) undoped ZnO and (*b*) $Zn_{0.98}Sr_{0.02}O$ nanostructures grown at 120°C deposition temperature and 350°C annealing temperature. (*B*) XRD patterns of ZnO nanostructures obtained at different growth temperature. Inset shows the change in lattice parameter (*a* and *c*) in the structures.

The internal structure of the films was examinedusing transmission electron microscopy (TEM) and high resolution TEM (HRTEM). Fig 2(*a*) shows TEM micrograph which confirms the formation of rod like structure in the SrZnO6 film which explains strong directional growth along [002] direction. HRTEM image (Fig 2(*b*)) of the same film indicates clear lattice fringes with *d*-spacing of 0.26 nm, corresponds to the (002) lattice plane of hexagonal ZnO. Energy Filtered Transmission Electron Microscopy (EFTEM) was done, to observe the distribution of the constituent element in the same Sr doped ZnO film. The green, red and violet color represent the distribution of Zn (Fig. 2(*c*)), Oxygen (Fig. 2(*d*)) and Sr (Fig. 2(*e*)), respectively. Homogeneous distribution of Zn and O is observed in the nanostructure.

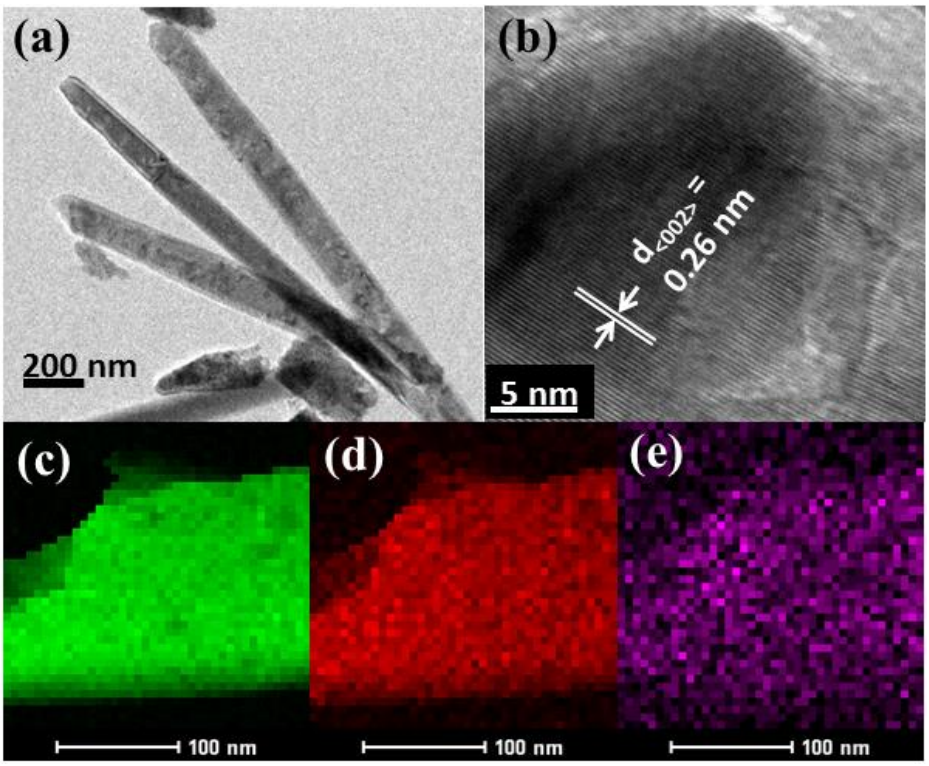

Fig. 2.(Color online)(a) HRTEM image and (b) lattice fringe of SrZnO6 nanostructure.(c-e) EFTEM elemental mapping, the green, red and violetcolor represent the distribution of Zn, O and Sr, respectively, within SrZnO6 nanostructure.

Variation of surface morphology with deposition temperature (DT) and annealing temperature (AT) of all the films is examined by FESEM. Figure 3(*a*-*h*) shows that all films surface consists of relatively nano-flower, uniform nano-rod and or nano-tube nanostructures with average length of 4-5 μm. All pure films are composed of nano-rod structure, whereas, at a fixed DT, ZnO films annealed at lower temperature (150°C) is denser and diameter of the nano-rods also slightly bigger compared to films annealed at higher temperature (~700 nm and ~550 nm for ZnO1 and ZnO3, respectively). Sr doped films shows different kind of morphology in comparison with the pure ZnO films. SrZnO1 and SrZnO3 both shows nano-flower type structures whereas, the size of the flower is less in SrZnO3 film(Fig 3(*e*-*f*)). Sr doped films deposited at 120°C do not shows any flower like surface structure; on the contrary it shows nano-tube like morphology (Fig 3(*g*-*h*)). Fig. 4(*a*-*e*) shows schematic of idealized and proposed formation mechanismsof ZnO crystal with different morphology.

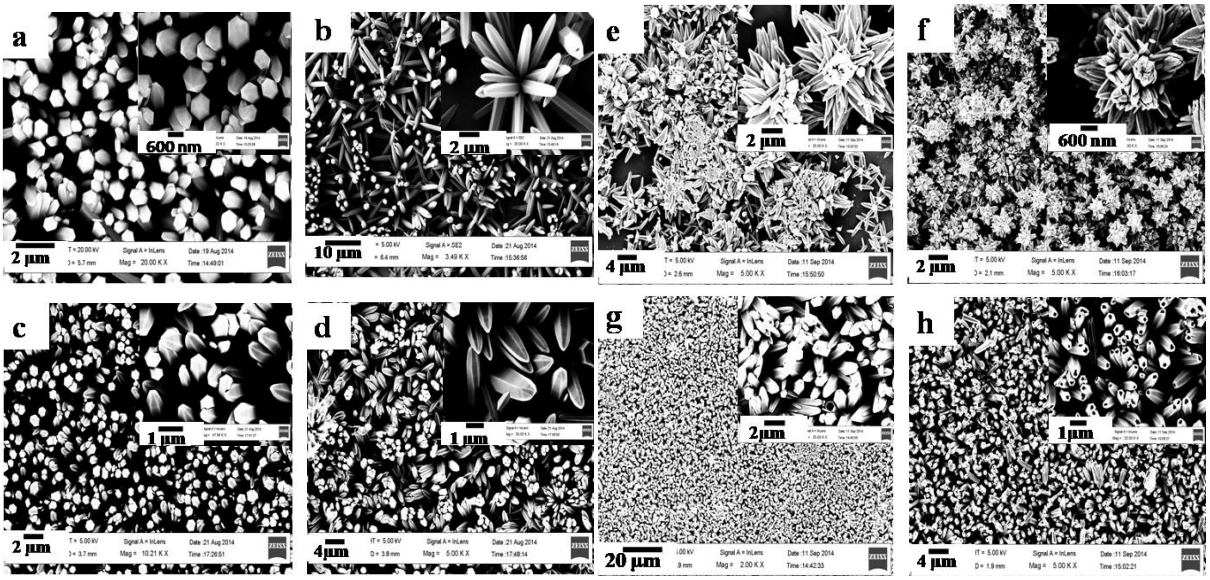

Fig. 3. SEM image of (*a*) ZnO1, (*b*) ZnO3, (*c*) ZnO4, (*d*) ZnO6, (*e*) SrZnO1, (*f*) SrZnO3, (*g*) SrZnO4 and (*h*) SrZnO6 nanostructures.

ZnO Nano structures growth mechanism:

The mechanism responsible for the growth of ZnO nanomaterials was $Zn(OH)_4^{2-}$ and $Zn(NH_3)_4^{2+}$as the growth units [13-14], in high pH solution, following the reactions from (1)-(7).

$$Zn(NO_3)_2 + 2H_2O \xleftrightarrow{NH_3,100°C\ /120°C} Zn(OH)_2 + 2HNO_3 \quad \text{--------- (1)}$$

$$Zn(OH)_2 \leftrightarrow Zn^{2+} + 2OH^- \quad \text{--------- (2)}$$

$$Zn^{2+} + 4NH_3 \leftrightarrow Zn(NH_3)_4^{2+} \quad \text{--------- (3)}$$

$$Zn^{2+} + 4OH^- \leftrightarrow Zn(OH)_4^{2-} \quad \text{--------- (4)}$$

$$Zn(OH)_4^{2-} \leftrightarrow ZnO + H_2O + 2OH^- \quad \text{-------- (5)}$$

$$ZnO + 2OH^- \leftrightarrow Zn(OH)_2 \leftrightarrow ZnO + 2H_2O \quad \text{-------- (6)}$$

$$Zn(NH_3)_4^{2+} + 2OH^- \leftrightarrow ZnO + 4NH_3 + 2H_2O \quad \text{-------- (7)}$$

The growth mechanism of different ZnO nano-structures (nano-belts, nano-combs, nano-springs, doughnut-shaped particles *etc.*) formation is still not very clear. Polar ZnO has a hexagonal closed packedstructure, each Zn^{2+} lies within a tetrahedral group of four oxygen ions, with polar axis along *c*-axis[15, 16]. ZnO exhibit several crystal planes (Fig 4(*a*)) different polarity (one polar zinc (0001) face, one basal polar oxygen $(000\bar{1})$ face, six nonpolar $(01\bar{1}1)$ faces and six symmetric nonpolar $(01\bar{1}0)$ faces parallel to *c*-axis)[14]. From the growth analysis of ZnO nanostructures synthesized by hydrothermal route, it is well accepted that in general relative growth velocity of the planes which determine the aspect ratio and the final shape of the ZnO is: $V_{<0001>} > V_{<01\bar{1}1>} > V_{<01\bar{1}0>} > V_{<000\bar{1}>}$ [16]. Plane, along which the crystal growth rate is maximum, disappears quicker in structure [14, 16]. Deposition temperature (DT) and annealing temperature (AT) both plays important role in controlling reaction rate as well as the structure formation. Initially, hexagonal shape nano-rods form due to slow growth of the $(01\bar{1}0)$ and higher growth rate along (0001) plane. With progress in the reaction, (*a*) concentration of growth unit reduces due to the deposition of ZnO and (*b*) equilibrium moves to the left (equ. 6 and 7) resulting a prominent dissolution effect. As the structure tries to minimize the surface energy, the dissolution rate of the polar (0001) plane, which has relatively higher surface energy, is faster than that of the nonpolar $(01\bar{1}1)$ and $(01\bar{1}0)$ planes [17]. Therefore, in slow reaction (low DT or AT) (0001) plane forms nano-rods with flat tip while for fast reaction (0001) plane disappears and $(01\,\bar{1}1)$ plane corresponds to the formation of the hexagonal needle shapetip as presented in Fig. 4(*b*-*c*).

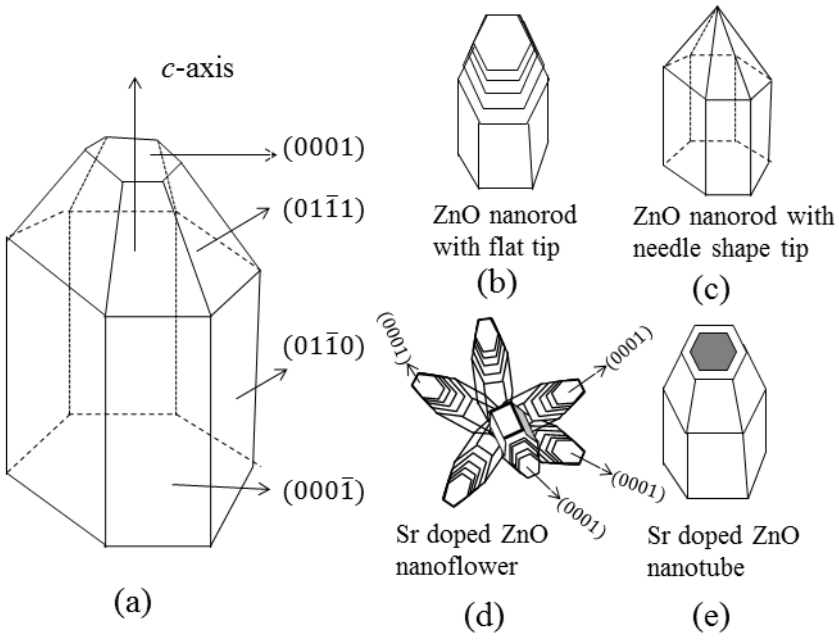

Fig. 4. Schematic diagram of the (*a*) Idealized; and proposed growth processes of nano-rod with (*b*) flat tip, (*c*) needle shape tip, (*d*) nano-flower and (*e*) nano-tube like ZnO structures

In Sr doped samples deposited at 100°C, secondary nucleation and growth of nano-flowers is observed which is very common in hexagonal ZnO, where circumferential edges have relatively higher free energies. It might be possible that in Sr doped solution the initial ZnO crystal has many polar (0001) surfaces leading to a flower shape structure formation as the reaction goes on along all the [0001] direction as drawn in Fig 4(*d*)[18]. Dissolution rate in the Sr doped samples deposited at 120°C is more prominent. Fig. 3 shows in SrZnO4 sample, small dissolution of the (0001) planes is observed in as-grown rods. As the annealing temperature increases, the wall thickness of the ZnO nano-rod becomes thinner, leading tothe formation of tubular ZnO tubes (Fig 4(*e*)).

RT Raman spectra's of ZnO and $Zn_{0.98}Sr_{0.02}O$ films are shown in Fig. 5. The phonon dispersion modes of the wurtzite ZnO structure, space group P63mc, can be decompose into 12 branches at the Γ point, $\Gamma = A_1 + E_1 + 2(B_1+E_2)$, whereas, $B_1$is infrared and Raman silent mode. Polar $A_1$and E_1 modeare infrared active therefore divided into transverse optical *(TO)* and longitudinal optical *(LO)* phonons. Non-polar E_2 is separated into E_2^{low} and E_2^{high} Raman active modes[19]. All these active Raman modes are very well assigned in the literature[19-22]. Decremps

etal.[20] reported six phonon frequencies, E_2^{low}, E_2^{high}, $A_1(TO)$, $E_1(TO)$, $A_1(LO)$ and $E_1(LO)$, at Γ point using Raman spectroscopy (at 99, 439, 382, 414, 574 and 580 cm^{-1}) and *ab* initio calculations (at 92, 449, 397, 426, 559 and 577 cm^{-1}) at ambient condition.Whereas, Serrano *et al.*[21] reported phonon frequency of two B_1 modes also along with the other six modes at 91, 261, 391, 409, 440, 552, 560 and 556 cm^{-1}.

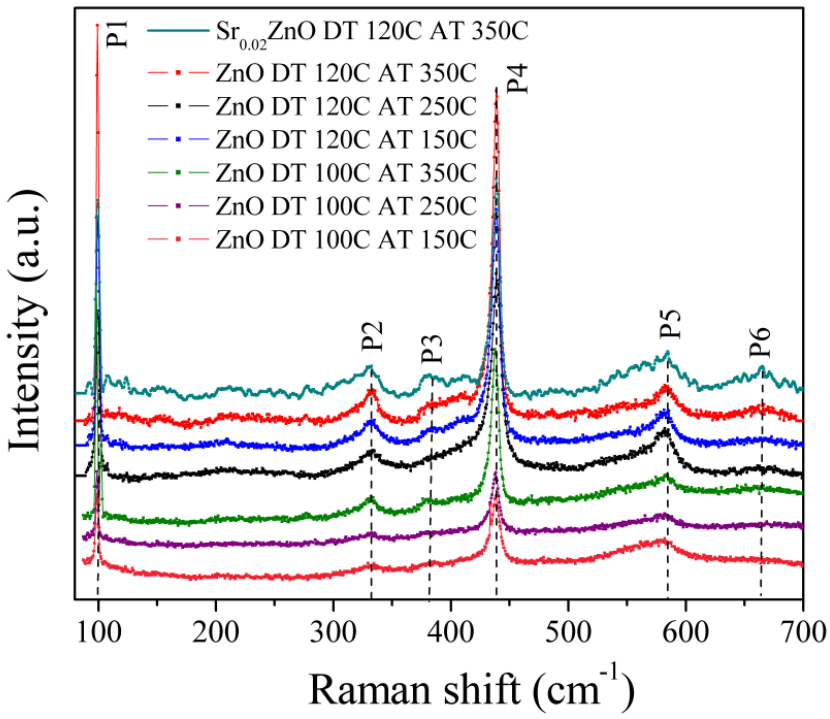

Fig. 5. (Color online)Room temperature Raman spectra of $Zn_{1-x}Sr_xO(x = 0\ and\ 0.02)$ nano structures.

In the present study, five phonon modes are observed for ZnO thin film at (P1) 99, (P2) 333, (P3) 382, (P4) 438 and (P5) 582 cm^{-1}. As shown in Fig. 5, Raman spectra of the films (ZnO1 to ZnO6 and SrZnO6) consists of high intensity non-polar E_2 optical mode at 99.3 (E_2^{low}) and 438.7(E_2^{high}) cm^{-1} and peak due to the multi-phonon process ($E_2^{high} - E_2^{low}$) at 332.3 cm^{-1}. Low intensity peak at 380.1 cm^{-1} is commonly assigned to A_1 (TO) mode of ZnO[12]. This peak is more prominent in the films annealed at 350°C and absent in the films annealed at 150°C. Bundesmann *et al.* [23]assignedthe peak at 583 cm^{-1}as a dopant defect peak in their report on different ion doped ZnO film. In our case, peak at 582 cm^{-1} is appeared in all the undoped as well as in doped ZnO films so we can eliminate the idea that this peak is due to defects creating from ion doping.

Intensity of this peak is very weak and broad for films deposited at 100°C but prominent for the films deposited at 120°C. Two LO modes of ZnO, situated at 575 (A_1(LO)) and 587 (E_1(LO)) cm^{-1} are allowed in $z(xx)z'$ and $x(zz)x'$ scattering configurations, respectively[23]. Weak feature of LO modes was previously reported for thin films and single crystals [19, 24, 25]. Therefore, the peak appeared at 582 cm^{-1} in all the films should be assigned to the combination of both LO vibrational modes of ZnO. In Sr doped film one weaker additional peak is observed at (P6) 633 cm^{-1}. Peak around this frequency is previously reported as effect of Zn_2MnO_4 spinal phase in Mn doped ZnO lattice [26, 27], or combined effect of A_1 (LO) + E_2^{low} and Zn_2MnO_4 precipitates [28] or due to oxygen vacancy [29]. In our report, low intensity peak at 663 cm^{-1} is absent in Raman spectra of pure ZnO films, so this can be assigned to only due to presence of Sr^{2+} ion in ZnO lattice. In order to check the application oriented optical capability of the nanostructures, effective phonon energy (E_{Ph}) is calculated using phonon mode position (E_i), FWHM (F_i) and the intensities (I_i) of the corresponding Lorentzian peaks,

$$E_{Ph} = \frac{\sum_i E_i F_i I_i}{\sum_i F_i I_i}$$

The effective phonon energy was calculated to be 490 and 453 cm^{-1} for the ZnO6 and SrZnO6 samples, respectively. The obtained value shows that Sr doping reduces the effective phonon energy, which is an important aspect for optical application as it minimizes nonradiative (multiphonon) losses.

RT UV–vis spectroscopic measurement of the nanostructures is carried out to study the effect deposition condition and Sr doping on the band gap of ZnO in the range of 300–800 nm. The UV-visible reflection spectra of ZnO3, ZnO6 and SrZnO6 nano structures are shown in Fig. 6. It is visible from Fig. 6 that ZnO grown in different deposition temperature shows no difference in reflection edge whereas a significant deviation is observed for 2% Sr doped samples towards higher wavelength. The band gap is 3.24 eV and 3.22 eV for the ZnO6 and SrZnO6 samples, respectively, which is calculated using the Tauc plot:

$$\alpha h\gamma = A(h\gamma - E_g)^n$$

where, α is the absorption coefficient, A is a constant, E_g is the band gap value and n is an unit less parameter with a value 2 or 1/2 for indirect or direct band gap semiconductors, respectively. Here

the decrease in the band gap in the doped samples attributes to the defects states generated in ZnO due to doping. Because of the formation of defect states in between the conduction and valance band of ZnO, when UV-vis light passes through the sample, energy required for the charge to flow is less compared to the pure ZnO sample.

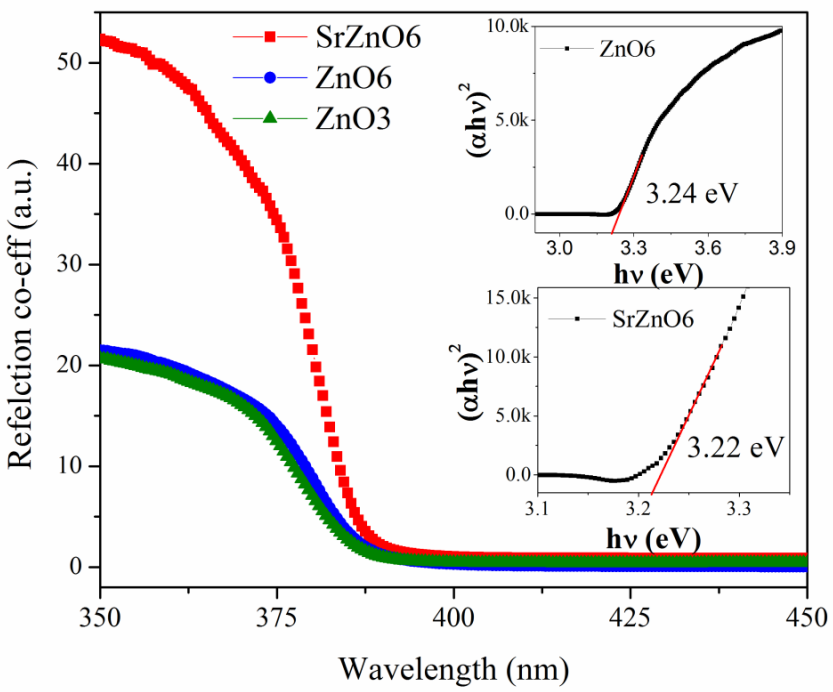

Fig. 6.(Color online)Room temperature UV–vis reflection spectra of $Zn_{1-x}Sr_xO$ ($x = 0$ *and* 0.02)nanostructures.

In contrastto the UV spectra, photoluminescence (PL) spectra of ZnO nanostructures are sensitive to the preparation procedure (in particular to the deposition and annealing temperature). With increase in the annealing temperature, band emission enhances remarkably but intensity of the green emission (near 2.2 eV) is independent of growth or annealing temperature (as shown in supplementary information). To understand the relative change in peak intensities with growth temperature, normalized PL emission spectra of the samples are plotted (Fig. 7(*a*)) over a broad range from 350 to 600 nm. As shown in Fig. 7(*a*), with increase in annealing temperature of pure ZnO, NBE peak position shifts toward higher energy side, whereas, the relative intensity of defect states especially in the blue-green region decreases noticeably keeping the defect peak position unchanged. However, it is important to notice that with Sr doping in the ZnO matrix replacing Zn,

(Inset of Fig. 7(*a*)) Zn defect related peak intensities decreases sharply which confirms Sr-substitution in ZnO lattice. In ZnO nanostructures, existence of defect states is very well known among which shallow Zn interstitials (Zn_{in}) and Oxygen vacancy (V_O) is mainly responsible for the green and yellow emission, as both have low formation enthalpies [30]. Apart from these, the existence of other intrinsic point defects and complexes (such as Zn vacancy (V_{Zn}), oxygen interstitials (O_{in}), antisite oxygen (O_{Zn}), complex of V_O and Zn_{in} (V_OZn_{in}) and complex of V_{Zn} and Zn_{in} ($V_{Zn}Zn_{in}$) have also been reported previously. The highest energy peak corresponds to the UV band edge emission is attributed to free exciton (FX) recombination through an exciton–exciton collision process[31]. As shown in Fig. 7(*a*), PL spectra of the samples grown at lower temperature (*ZnO1, ZnO3, and ZnO4 films*) are shifted towards lower binding energy. This might be because of the higher defect levels in these films due to which emission in between swallow acceptor and donor levels overcomes the free exciton emission intensity making it difficult to obtain the actual free excitonic emission wavelength.

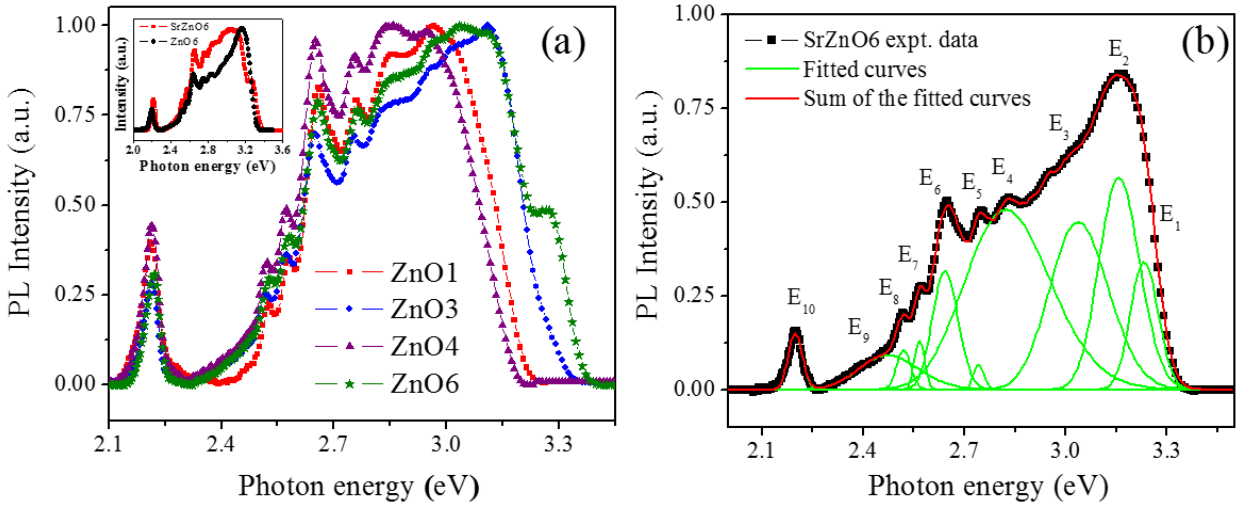

Fig. 7. (Color online) (*a*) Room Temperature normalized PL spectra of ZnO and inset shows the Spectra of $Zn_{1-x}Sr_xO(x = 0\ and\ 0.02)$ nanostructures. (*b*) Normalized PL spectra of SrZnO6 nanostructure. The "■" shows experimental data. Solid green and red lines are Gaussian fitting of individual peaks and sum of all peaks, respectively.

Therefore, for a detail understanding wide emission spectrum of SrZnO6 nanostructure extending from near band edge (NBE) to green emission is well resolved into 10 Gaussian peaks (Fig. 7(*b*))

and Fig. 8(*a*) illustrates the schematic band diagram of all the emissionsconstructed from the PL data. First peak (E_1) at 3.23 eV in the UV regioncorresponds to the near band emission (NBE) in ZnO film [31, 32]. Second emission peak (E_2) with an energy difference of 79 meV with E_1, located at 3.15 eV, is reported to be attributed to the first longitudinal optical (LO) phonon replica of FX which is very close to the previous reported energy difference (72 meV) between two corresponding LO-phonon replicas [33]. Theoretical prediction shows that Zn_{in} defect level lies ~0.15 to 0.22 eV below the minima of conduction band (CB)[34, 35]. Therefore the third, violet-blue emission peak (E_3) at 3.0 eV, is believed to be originated from the swallow doner, Zn_{in} to valance band (VB). Broad blue emission peak (E_4) centered at 2.82 eV is originated due to recombination of electron and hole in between CB and O_{in} level which lies 0.4 eV above the VB maxima[22]. A small peaks located at 2.72 eV (E_5) originated due to recombination of electron and hole in between Zn_{in} and shallow acceptor V_{Zn}, lies ~0.1 eV below the O_{in} level[22]. Another blue emission peak (E_6) located at 2.62 eV was attributed to the electron transition from Zn_{in} to O_{in} acceptor level. Studies revealed that the green emission in ZnO is strongly related to the oxygen-related defects in theZnO[36]. The wide green emission range in the Sr doped nanostructure can be divided into several peaks. Fig. 7(b) shows three prominent peaks, E_7, E_8 and E_9 at 2.56, 2.52 and 2.46 eV, respectively. Erhart *et al.* showed an oxygen vacancy related transition at ~0.7 eV below the calculated CB minima [34]. Calculation based on full potential linear muffin-tin orbital method explained that the position of the oxygen vacancies (V_O) level is located approximately at 2.46 eV below the CB [37]. So these three emissions are attributed to CB or deep level or trap-state to oxygen singly charged $V_O$defect state[38]. Following the band diagram reported by Behera *et al.*, yellow luminescence peak at 2.20 eV (E_{10}) is originated due to antisite oxygen (O_{Zn}) defect state [22].

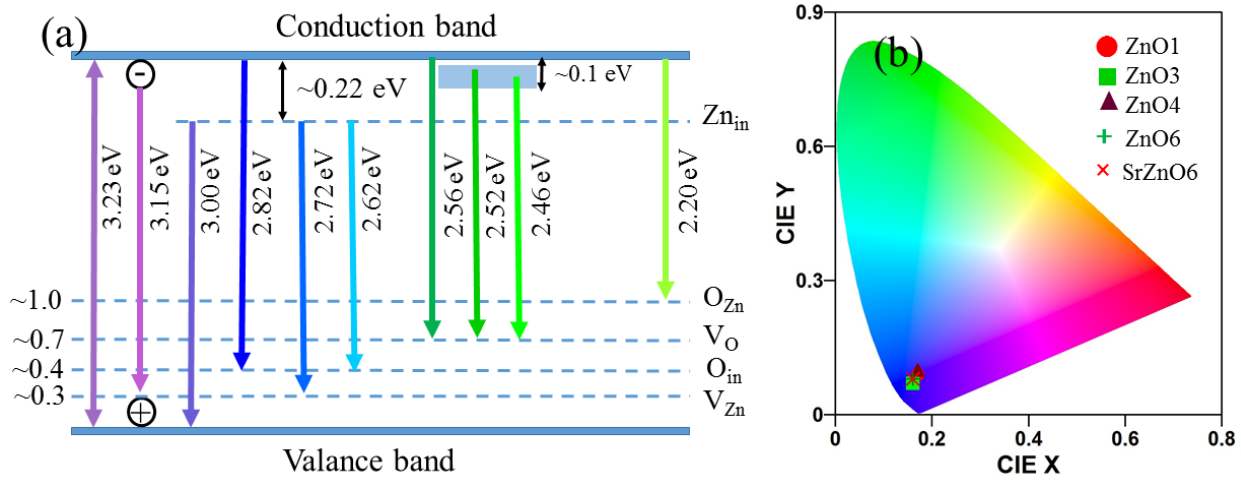

Fig. 8. (Color online) (*a*) Schematic band diagram of Sr doped ZnO nanostructure deposited at 120°C and annealed at 350°C and (*b*) The CIE diagram of doped and undoped ZnO nanostructures.

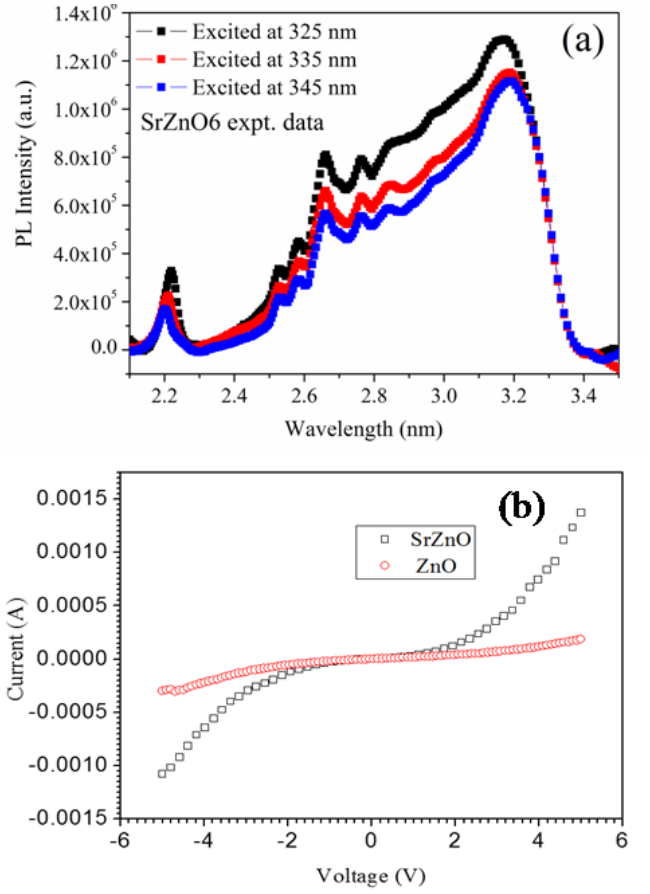

Fig. 9. (Color online) (a) Room temperature PL spectra for different excitation wavelengths and (b) Current –Voltage characteristics of ZnO and Sr doped ZnO nanostructures.

Figure 8(*b*) shows the CIE (International Commission on Illumination) color space chromaticity diagram, plotted using the Colour calculator software, in the (x, y) coordinates system. The chromaticity coordinates are (0.17, 0.09), (0.16, 0.07), (0.17, 0.10), (0.16, 0.08) and (0.16, 0.08) for ZnO1, ZnO3, ZnO4, ZnO6 and SrZnO6 nanostructures, respectively which indicate a strong blue PL CIE shade for all the samples.

In order to illustrate the emission characteristics and the excitation wavelength dependence, PL emissions of SrZnO6 nanostructure for three different excitation wavelengths is been plotted

(Fig 9(a)). Materials containing defect levels, might show different PL spectra upon exciting with different excitation energy due to the contribution from defect levels. The emission results show no spectral shift under different UV excitations and gives stable emission peak color, which is favourable for many optoelectronic applications.

Fig. 9(b) depict the current–voltage (I–V) characteristics for ZnO and SrZnO. The *I–V* characteristics appear to be symmetric with respect to the bias. Consistent and precise results could only be obtainedwith a combination of Ohm's law for low voltages, as Ohm's law is usually valid for the low-voltage – intrinsic – regime of a low-conductivity material [39]. The entire *I-V* characteristics reveal good rectification behaviour of the Schottky diodes. The current in reverse bias and forward bias is higher in Sr doped ZnO samples compared to ZnO samples, indicating increase in carrier concentration by Sr doping.

4. Conclusions

We have successfully synthesized Sr doped and pure ZnO nanostructures on glass substrates by hydrothermal synthesis. Decrease in the theta value of XRD peaks confirms Sr substitution in the ZnO lattice. FESEM reveals that shape of the ZnO nanostructures strongly depends on the growth temperature.The XRD and TEM confirms that ZnO nanostructures possess good crystalline structures with growth direction along the *c*-axis of the crystal plane. Compared with the conventional autoclave heating and microwave irradiation synthesis, our technique is much simpler, cost effective and quick way to obtain significantly better regular arranged nano-rods (pure ZnO) and nano tubes/flower in Sr doped ZnO. Raman spectra of all the nanostructures show five characteristics phonon dispersion peak of wurtzite ZnO, while one additional peak at 663 cm^{-1} is observed in the Sr doped ZnO sample which is assigned to the intrinsic defects created in the ZnO matrix due to Sr doping. Room temperature UV–vis spectroscopy measurements show decrease in the band gap energy in the Sr doped samples while it is same for pure ZnO prepared in different deposition temperatures. PL spectra shows, Zn and Oxygen defect state intensities in the pure ZnO structures decreases and NBE shifts towards higher energy with increase in growth temperature. Moreover, the Sr doping at Zn is found to be favorable to decrease Zn vacancy defects in the structure and excitation wavelengths dependent measurement establishes it suitable for many

optoelectronic applications. I-V characteristics of the ZnO and Sr doped ZnO shows rectification behaviour of the Schottky diodes.

Acknowledgments

This work was supported by the Department of Science and Technology, India by awarding the prestigious 'Ramanujan Fellowship' (SR/S2/RJN-121/2012) to the PMS. PMS is thankful to Prof. Pradeep Mathur, director, IIT Indore, for encouraging the research and providing the necessary facilities. We are thankful to Dr. Vasant Sathe, IUC-DAE Consortium for Scientific Research, Indore for his help to do Raman measurement of the samples. The authors thankful to SIC at IIT Indore for providing the characterization facilities. The help received from, Dr. Anjan Chakraborty, Mr. Kinny are also acknowledged.

References

1 G. A. Prinz, *Science*, 1998, **282**, 1660.

2 D. G. Thomas, *J. Phys. Chem. Solids*,1960, **15**, 86.

3 D. C. Reynolds, D. C. Look, B. Jogai, C. W. Litton, G. Cantwell and W. C. Harsch, *Phys. Rev. B*, 1999, **60**, 2340.

4 D. M. Bagnall, Y. F. Chen, Z. Zhu, T. Yao, S. Koyama, M. Y. Shen and T. Goto, *Appl. Phys. Lett.*,1997, **70**, 2230.

5 D. C. Look, *Mater. Sci. Eng. B*, 2001, **80**, 383.

6 H. Zhang, D. Yang, Y. Ji, X. Ma, J. Xu and D. Que, *J. Phys. Chem. B*,2004, **108**, 3955.

7 X. P. Gao, Z. F. Zheng, H. Y. Zhu, G. L. Pan, J. L. Bao, F. Wu and D. Y. Song, *Chem. Comm.*, 2004, **12**, 1428.

8 B. Liu, S. H. Yu, F. Zhang, L. J. Li, Q. Zhang, L. Ren and K. Jiang, *J. Phys. Chem. B*, 2004, **108**, 4338.

9 F. Li, Y. Ding, P. X. Gao, X. Q. Xin and Z. L. Wang, *Angew. Chem., Int. Ed.*, 2004, **43**, 5238.

10 J. Liang, J. Liu, Q. Xie, S. Bai, W. Yu and Y. Qian, *J. Phys. Chem. B*, 2005,**109**,9463.

11 J. B. Wang, G. J. Huang, X. L. Zhong, L. Z. Sun, Y. C. Zhou and E. H. Liu, *Appl. Phys. Lett.* , 2006,**88**,252502.

12 J. Zhao, X. Yan,Y. Lei, Y. Zhao, Y. Huang and Y. Zhang, *Advances in Materials Research*, 2012, **1**, 75.

13 S. Cho, S.-H.Jung and K.-H. Lee, *J. Phys. Chem. C*,2008,**112**, 12769.

14 Y. Fang, Q. Pang, X. Wen, J. Wang and S. Yang, *Small*, 2006, **2**, 612.

15D. Wang and C. Song,*J. Phys. Chem. B*, 2005,**109**, 12697.

16 W. J. Li, E. W. Shi, W. Z. Zhong and Z. W. Yin, *J. Cryst. Growth*,1999, **203**, 186.

17 A. Wei, X. W. Sun, C. X. Xu, Z. L. Dong, Y. Yang, S. T. Tan and W. Huang, *Nanotechnology*, 2006, **17**,1740.

18 R. A. McBride, J. M. Kelly and D. E. McCormack, *J. Mater. Chem*., 2003, **13**, 1196.

19 N. Ashkenov, B.N. Mbenkum, C. Bundesmsnn, V. Riede, M. Lorentz, D. Spemann, E.M. Kaidashev, A. Kasic, M. Schubert, M. Grundmann, G. Wagner, H. Neumann, V. Darakchieva, H. Arwin and B. Monemar, *J. Appl. Phys.*,2006, **93**, 126.

20 F. Decremps, J. Pellicer-Porres, A.M. Saitta, J.-C.Chervin, and A.Polian, *Phys. Rev. B*,2002, **65**, 092101.

21 J. Serrano, A. H. Romero, F. J. Manjon, R. Lauck, M. Cardona and A. Rubio, *Phys. Rev. B*,2004,**69**, 094306.

22 D. Behera and B.S. Acharya, *Journal of Luminescence*, 2008, **128**, 1577.

23 C. Bundesmann, N. Ashkenov, M. Schubert, D. Spemann, T. Butz, E. M. Kaidashev, M. Lorenz and M. Grundmann, *Appl. Phys. Lett.*,2003, **83**, 1974.

24 E. F. Venger, A. V. Melnichuk, L. Lu. Melnichuk and Yu. A. Pasechnik, *Phys. Status Solidi B.*,1995, **188,** 823.

25 B. H. Bairamov, A. Heinrich, G. Irmer, V. V. Toporov and E. Ziegler, *Phys. Status Solidi B*, 1983, **119**, 227.

26 T. L. Phan, R. Vincent, D. Cherns, N. X. Nghia, M. H. Phan and S–C. Yu, *J. Appl. Phys*.,2007, **101**, 09H103.

27 H. Y. Xu, Y. C. Liu, C. S. Xu, Y. X. Liu, C. L. Shao and R. Mu, *J. Chem. Phys.*, 2006, **124**, 074707.

28 J. B. Wang, H. M. Zhong, Z. F. Li and W. Lu, *J. Appl. Phys.*, 2005, **97**,086105.

29 L. W. Yang, X. L. Wu, G. S. Huang, T. Qiu and Y. M. Yang, *J. Appl. Phys.*, 2005, **97**, 014308.

30 S. B. Zhang, S. H. Wei and A. Zunger, *Phys. Rev. B*, 2001,**63**,075205.

31 K. Y. Wu, Q. Q. Fang, W. N. Wang, C. Zhou, W. J. Huang, J. G. Li, Q. R. Lv, Y. M. Liu, Q. P. Zhang and H. M. Zhang, *J. Appl. Phys.*,2010, **108**, 063530.

32 A. S. H. Hameed, C. Karthikeyan, S. Sasikumar, V. S. Kumar, S. Kumaresan and G. Ravi, *J. Mater. Chem. B*, 2013, **1**, 5950.

33 X. Meng, Z. Shi, X. Chen, X. Zeng and Z. Fu, *J. Appl. Phys.*,2010, **107**, 023501.

34P. Erhart, K. Albe and A. Klein, *Phys. Rev. B*, 2006, **73**, 205203.

35 N.H. Alvi, K.U. Hasan, O. Nur and M. Willander, *Nanoscale Res. Lett.*,2011, **6**, 130.

36 S.B. Zhang, S.H. Wei and A. Zunger, *Phys. Rev. B*, 2001, **63**, 075205.

37 C. Ahn, Y.Y. Kim, D.C. Kim, S.K. Mohanta and H. K. Cho, *J. Appl. Phys*.,2009, **105**,013502.

38 T. M. Børseth, B. G. Svensson, A. Y. Kuznetsov, P. Klason, Q. X. Zhao and M. Willander, *Appl. Phys. Lett.*, 2006, **89**, 262112.

39 M. A. Lampert and P. Mark, Current Injection in Solids,*Academic Press*, *New York*, 1970.